First-principles density functional theory study of native point defects in Bi_2Te_3

Adham Hashibon[*] and Christian Elsässer

Fraunhofer-Institut für Werkstoffmechanik IWM, Wöhlerstraße 11, D-79108 Freiburg, Germany

(Received 16 July 2011; revised manuscript received 6 October 2011; published 27 October 2011)

We present a first-principles study of the native point defects in the thermoelectric material Bi_2Te_3. Calculated formation energies of defects and electronic densities of states were analyzed in detail. The most prominent native point defects considered are vacancies and antisite defects on the Bi, Te1, and Te2 sublattices of the Bi_2Te_3 structure. Vacancies on all three sublattices are found to have much higher formation energies than antisite defects. The most dominant antisite defects are found to be Bi_{Te1} at Bi-rich conditions, and Te_{Bi} at Te-rich conditions. These lead to the formation of resonant defect states at the top of the valence band and bottom of the conduction band, respectively. Hence they are expected to impact charge and energy transport in a profound way. Furthermore antisite defect pairs tend to form at nearest-neighbor distances, and lead to substantial changes in the electronic structure and hence in the thermoelectric properties of Bi_2Te_3.

DOI: 10.1103/PhysRevB.84.144117 PACS number(s): 77.22.Ej, 31.15.A−, 84.60.Bk

I. INTRODUCTION

Some of the best thermoelectric materials known for applications at room temperature are based on Bi_2Te_3 and its alloys, such as $Bi_{2-x}Sb_xTe_3$ and $Bi_2Te_{3-x}Se_x$ (see, e.g., Refs. 1 and 2). The energy conversion efficiency of a thermoelectric material is typically characterized by the dimensionless figure of merit $ZT = S^2\sigma T/\kappa$, where S is the Seebeck coefficient, σ is the electrical conductivity, κ is the thermal conductivity, and T is temperature. Substantial efforts have been made to enhance the thermoelectric properties of Bi_2Te_3-based thermoelectric materials in order to get the figure of merit ZT at room temperature increased to more than 1. Such efforts are by chemical synthesis of bulk nanostructured materials with a precise control of the composition,[3–6] or by various thin-film deposition techniques.[7–10] A prerequisite for optimal thermoelectric performance is materials with well-defined electrical and thermal conductivities, high mobility of free current carriers, and thermoelectric power. However, these properties are influenced by the presence of impurities and their interaction with native point defects. Therefore the investigation of the nature of native point defects in Bi_2Te_3 is vital both for an understanding of the thermoelectric properties and for their optimization for practical devices.

Bi_2Te_3 is a narrow-band-gap semiconductor ($E_g = 0.13$ eV[11]) having a tetradymite crystal structure with the space group $R\bar{3}m$. The rhombohedral primitive unit cell contains two nonequivalent sites for the Te atoms, Te1 and Te2, and one for the Bi atoms; see Fig. 1(a). The conventional hexagonal unit cell shown in Fig. 1(b) contains three formula units of Bi_2Te_3 and exhibits the layered crystal structure of tetradymite materials. The fundamental building block is composed of five atomic layers in the sequence [Te1-Bi-Te2-Bi-Te1]; these are repeated periodically along the c axis, as shown in Fig. 1(b). The Te1-Te1 interaction is commonly assumed to be of the van der Waals type[12] and is characterized by a large interatomic separation (3.66 Å compared to 3.25 Å and 3.07 Å[13] for Bi-Te2 and Bi-Te1, respectively).

Deviations from stoichiometry or the presence of impurities have been shown to affect the type, density, and mobility of charge carriers and hence also the thermoelectric properties of Bi_2Te_3-based materials.[6,7,14–17] In particular, the nature of the carrier type was found to be strongly dependent on intrinsic point defects, leading to intensive efforts to understand the role of these defects in variation of the thermoelectric properties.[5,7,10,14–16,18–23]

Consistent with the general behavior of $A_2^VB_3^{VI}$ semiconductors, Bi_2Te_3 crystals grown from stoichiometric melts show an enhanced overstoichiometry of the group-V element. Excess Bi can be accommodated in single-crystalline Bi_2Te_3 by means of the following point-defect mechanisms: (i) antisite (AS) defects, i.e., by replacement of Te atoms on a Te sublattice by Bi atoms, denoted as Bi_{Te}; (ii) by additional regular Bi sites, i.e., Bi_{Bi}, accompanied by the creation of vacancies on a Te sublattice, denoted as V_{Te}; (iii) by interstitial Bi atoms. On one hand, Miller and Li[19] found, based on high-precision density measurements, that stoichiometric Bi_2Te_3 has 62.8 at. % Te content, and that the crystals were p type, in agreement with the phase diagram found by Satterthwaite *et al.*,[18] On the other hand, da Silva *et al.*,[23] found that a 60 at. % Te is sufficient to result in n-type conduction, and that higher concentrations of Te could not be maintained as it evaporated from their lattices. This indicates a strong dependence of the concentration and mechanism of antisite defects on the chemical environment.

Furthermore, Miller and Li[19] found that the dominant point defects for Bi-rich conditions were Bi_{Te} antisite defects, confirming the earlier suggestion of Harman *et al.*,[24] and that interstitials of Bi and vacancies of Te were unlikely to appear. For Te-rich samples, their results further suggest that antisite defects may still be favorable although did not exclude vacancies. The work of Satterthwaite *et al.*,[18] Brebrick,[20] and more recently of Cho *et al.*[10] proposed that singly ionized Bi_{Te} and Te_{Bi} antisite defects are present at Bi-rich and Te-rich conditions as acceptors and donors, respectively, and they accounted for the charge carrier concentration assuming solely these two defects. Since more Te sites than Bi sites exist in the lattice (3:2 ratio), it is expected that there will be a bias toward an excess of Bi_{Te} defects, leading in most cases to p-type semiconduction.

Point-defect models suggested by Drašar, Bludská, Lošt'ák, *et al.*,[14–16] which are based on Hall-effect measurements, assume that overstoichiometric Bi should be accommodated by the formation of vacancies of Te, V_{Te}, in addition to

 ©2011 American Physical Society

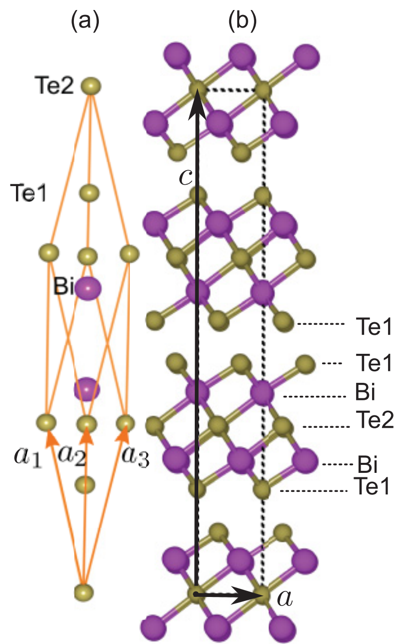

FIG. 1. (Color online) (a) The rhombohedral primitive and (b) the hexagonal conventional unit cells of Bi_2Te_3.

Bi_{Te} defects and in order to satisfy charge balance, vacancies of Bi, V_{Bi}, were also assumed to form. Frangis *et al.*,[25] suggested a qualitatively different model to accommodate overstoichiometry. Based on high-resolution transmission electron microscopy they observed, in addition to the five-layer lamella structures, lamellae of seven and nine layers, which are characterized by an addition of one or two Bi-Te pairs into the five-layer structure, respectively. This mechanism is equivalent therefore to a defect model which excludes the formation of vacancies.

All the above models do not take into account explicitly the energy costs associated with creating each of these point defects. Furthermore, although most studies suggest that antisite defects are more likely to be found on the Te1 sublattice, no direct calculation of the formation energy was reported so far, hence no distinction could be made between AS on the Te1 or Te2 sublattices. However, it is believed that vacancies on the Te1 sites are more favorable due to the large van der Waals gap, hence they are assumed to be dominating. The concentration of native defects depends on the formation energy by the well-known expression of statistical mechanics:[26] $c \propto \exp(-E_f/K_BT)$, where c is the defect concentration, E_f is the defect formation energy, and k_B is Boltzmann's constant; knowledge of the formation energies is vital for a better understanding of native doping mechanisms and the possible role of point defects for thermoelectric properties in Bi_2Te_3. Nevertheless, information on the formation energies is scarce. Horák *et al.*,[19,22] have estimated experimentally the formation energy of Bi_{Te} under Bi-rich conditions to be about 0.4 eV, which is substantially smaller than typical vacancy formation energies which are usually of the order of 1 eV. Theoretical studies of Pecheur and Toussaint,[27] based on a tight-binding model, suggested that Bi_{Te} antisite defects are favorable, but they did not give any estimates for the formation energy. First-principles density functional theory calculations of Thonhauser *et al.*,[28] on the closely related compound Sb_2Te_3 did include a calculation of vacancy and antisite defect formation energies. They showed that in Sb_2Te_3, the defects with lowest formation energy are the antisite Sb_{Te1}, while vacancy formation energies are well above 1 eV. However, they did not consider the effect of the chemical environment, which is expected to be significant.[29]

In order to determine which of the point-defect types are most probable at various experimental conditions, and hence most relevant for the optimization of the thermoelectric properties, it is necessary to know the formation energies of the various defects, and their dependence on the chemical environment, as characterized by chemical potentials. In the present study, we investigate the formation of point defects in Bi_2Te_3 by first-principles calculations based on the density functional theory (DFT). Vacancies and stoichiometric as well as nonstoichiometric antisite defects are considered, taking into account the variation of chemical potentials. We also analyze the electronic structure of the point defects and their doping mechanism, i.e., their contribution to charge carrier type and mobility.

This paper is organized as follows: In Sec. II we describe the point defects considered in this study and the details of the computational approach. In Sec. III, the results of our calculations of formation energies for the vacancy and antisite defects are presented and discussed. The paper is concluded in Sec. IV.

II. THE MODEL SYSTEM

The calculations of formation energies are performed assuming the dilute limit of point defects using a supercell setup with periodic boundary conditions (PBCs) in all directions. Introducing a point defect into the conventional hexagonal unit cell shown in Fig. 1(b), for example, by replacing one Bi atom for Te to obtain a Bi_{Te1} antisite defect, would be equivalent to replacing a whole layer of Te1 atoms by Bi, which would result in a completely different structure. In the present study we use a hexagonal $2 \times 2 \times 1$ supercell model for our calculations, which is produced by repeating twice the hexagonal conventional unit cell in the two directions of the basal plane. The resulting supercell, shown schematically in Fig. 2, is composed of 12 formula units of Bi_2Te_3, i.e., 24 Bi and 36 Te atoms.

Introducing a single point defect in this system results in a distribution of isolated point defects, where the rest of the periodic images of each defect are separated laterally by a distance of $2a$, where a is the basal lattice parameter of the hexagonal conventional unit cell. The experimental lattice parameters are given in Table I.

The employed PBCs lead inherently to a finite interaction energy between each defect and all its images. This interaction energy cancels out only in the limit of an infinite system. In order to estimate this interaction energy for a finite system, and the influence of system size on the calculated formation energies, one normally performs several calculations with increasing system size and separation of the point defects. Since the hexagonal $2 \times 2 \times 1$ unit cell used in this study is already large, for the sake of computational efficiency

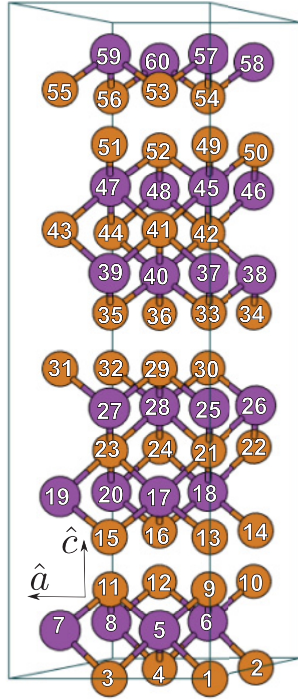

FIG. 2. (Color online) The hexagonal $2 \times 2 \times 1$ supercell used for the calculations of the point defects. Indexes are attached to the different atoms to facilitate identification of point defects. In each layer, smaller indices indicate atoms nearer to the observer.

we instead introduce an additional defect into the hexagonal $2 \times 2 \times 1$ supercell, and calculate the formation energy at various distances between the pairs of defects within the same hexagonal $2 \times 2 \times 1$ supercell.

Calculations are performed for the most prominent defects in Bi_2Te_3, namely vacancies on the Bi, Te1, and Te2 sublattices, denoted as V_{Bi}, V_{Te1}, and V_{Te2}, respectively, and antisite defects on the Bi, Te1, and Te2 sublattices, denoted as Te_{Bi}, Bi_{Te1}, and Bi_{Te2}, respectively. By introducing these defects individually into the hexagonal $2 \times 2 \times 1$ supercell

TABLE I. Lattice parameters as calculated in this study for Bi (rhombohedral, space group $R\bar{3}m$), Te (trigonal phase, space group $P3_121$), and Bi_2Te_3, compared to experimental data and other theoretical calculations.

		a (Å)	c/a	u_{Bi}	v_{Te}
Bi					
	This work	4.538	2.548	0.233	
	Ref. 30	4.474	2.594	0.234	
	Exp. (Ref. 31)	4.535	2.611	0.234	
Te					
	This work	4.308	1.373		0.292
	Ref. 32	4.302	1.380		0.291
	Ref. 33	4.280	1.376		0.287
	Exp. (Ref. 34)	4.451	1.331		0.263
Bi_2Te_3					
	This work	4.390	6.783	0.400	0.209
	Ref. 35	4.530	6.761	0.400	0.209
	Exp. (Ref. 13)	4.384	6.955	0.400	0.212

the overall stoichiometry of the system is altered. Similarly to Ref. 28 we consider in addition a third type of defect created by exchanging the positions of two atoms with opposite types within the supercell. Two kinds of these so-called exchange pairs are possible, depending on whether a Bi atom is exchanged with a Te atom on the Te1 or Te2 sublattices, denoted as $X_{Bi\text{-}Te1}$ and $X_{Bi\text{-}Te2}$, respectively. Such exchange-pair defects are equivalent to introducing two opposite antisite defects, i.e., a Bi_{Te1} and a Te_{Bi}, in the case of $X_{Bi\text{-}Te1}$ or a Bi_{Te2} and a Te_{Bi} in the case of $X_{Bi\text{-}Te2}$, and therefore do not affect the stoichiometry of the system.

Depending on which atoms are being exchanged, the two antisite defects composing the exchange pair may be at different separations. Hence a direct estimation of the interaction between the antisite defects of opposite types can thus be estimated.

A. Details of the computational method

The first-principles method used in the present study is based on DFT. Calculations of total energies and electronic structures are done by means of the computational mixed-basis pseudopotential (MBPP) method[36–38] employing the local-density approximation for exchange and correlation (LDA)[39,40] and norm-conserving pseudopotentials.[41] Pseudopotentials for both Bi and Te were constructed from all-electron valence states for free atoms according to Ref. 42. Atomic reference configurations that include the semicore d states in the valence orbitals were used: Bi($5d^{10}6s^26p^3$) and Te($4d^{10}5s^25p^4$). A second set of pseudopotentials without inclusion of the semicore d states in the valence was also considered. However this failed to reproduce the layered structure because the Te1-Te1 interatomic distance was severely underestimated. A mixed-basis was used with plane waves up to a cutoff energy of $E_{pw} = 16$ Ry (1 Ry = 13.606 eV) and localized functions confined to atom-centered spheres with radii $R_{l0} = 2.5$ bohrs for d semicore states of Bi and Te (1 bohr = 0.529 Å).

For the hexagonal $2 \times 2 \times 1$ Bi_2Te_3 systems, the intensive calculations of formation energies, which include relaxation of all atomic positions, were performed with a $2 \times 2 \times 1$ Monkhorst-Pack mesh.[43] The calculations of lattice parameters and total energies of elemental Te (space group $P3_121$) were performed using the hexagonal primitive unit cell containing 3 atoms. For the corresponding calculations for elemental Bi (space group $R\bar{3}m$) the hexagonal conventional unit cell containing three formula units (6 atoms) was used instead of the rhombohedral primitive unit cell. Since all systems are represented by hexagonal unit cells, maximum cancellation of errors in energy differences can be achieved by choosing, as much as possible, equivalent k-point meshes in all systems. This can be obtained by scaling the k-point meshes according to the size of the Brillouin zones of the corresponding systems. For Te a $4 \times 4 \times 5$ k-point mesh and for Bi a $4 \times 4 \times 3$ k-point mesh result in the best equivalence with the hexagonal $2 \times 2 \times 1$ Bi_2Te_3 system. For the electronic structure calculations a $6 \times 6 \times 1$ k-point mesh was used for the hexagonal $2 \times 2 \times 1$ Bi_2Te_3 system. For comparison, a rhombohedral Bi_2Te_3 unit cell with $12 \times 12 \times 12$ k-point mesh was also used for bulk DOS calculations. For the

determination of the Fermi level a Gaussian smearing by 0.2 eV was used.[44,45] These k-point settings led to sufficient convergence of differences in total energies to less than 0.05 eV/atom. The site- and angular-momentum-projected densities of states (PDOSs) were calculated by integrating the wave functions in atom-centered spheres of radius 2.5 bohrs, which is approximately half of the nearest-neighbor distance between the atoms. A Gaussian broadening of 0.1 eV full width at half maximum (FWHM) was applied to the discrete energy eigenvalues of the k-point mesh.

B. Calculation of the formation energy

The formation energy of a point defect E_f is calculated according to the *ab initio* thermodynamics approach[29] by the equation

$$E_f = E_{\mathrm{tot}}^{\mathrm{def}} - E_{\mathrm{tot}}^{\mathrm{bulk}} - \sum_i \Delta n_i \mu_i - q(\epsilon_v - \epsilon_F), \qquad (1)$$

where $E_{\mathrm{tot}}^{\mathrm{def}}$ and $E_{\mathrm{tot}}^{\mathrm{bulk}}$ are the total energies of the supercell with and without a defect, respectively. Δn_i is the change in the number of atoms of species i, i.e., of either Bi or Te, in the unit cell relative to the ideal bulk one. The μ_i is the chemical potential of the element i. The last term gives the variation in the energy due to the charge state of a defect. In the present study, due to the small band gap of Bi_2Te_3 only charge neutral defects are considered and therefore this term is neglected. See Refs. 29,46, and 47 for more specific details.

In previous calculations by Thonhauser *et al.*[28] for the closely related system of Sb_2Te_3, the chemical potentials in Eq. (1) were considered to be total energies of ideal elemental bulk Bi and Te crystals. This implies that the system is at the same time in equilibrium with both a Bi-rich and a Te-rich phase. In this work a more realistic assumption is made, whereby the system is in equilibrium with a bulk Bi_2Te_3 reservoir. Hence the chemical potentials of Bi and Te are related through

$$\mu_{\mathrm{Bi_2Te_3}}^{\mathrm{bulk}} = 2\mu_{\mathrm{Bi}} + 3\mu_{\mathrm{Te}}, \qquad (2)$$

where $\mu_{\mathrm{Bi_2Te_3}}^{\mathrm{bulk}}$ is the chemical potential of one formula unit of Bi_2Te_3. The Gibbs free energy of formation of one formula unit of Bi_2Te_3 is given as

$$\Delta G^0(\mathrm{Bi_2Te_3}) = \mu_{\mathrm{Bi_2Te_3}}^{\mathrm{bulk}} - 2\mu_{\mathrm{Bi}}^0 - 3\mu_{\mathrm{Te}}^0. \qquad (3)$$

From Eqs. (2) and (3), the following expression for the formation energy as a function of $\Delta\mu_{\mathrm{Te}} = \mu_{\mathrm{Te}} - \mu_{\mathrm{Te}}^0$ is obtained, where μ_{Te}^0 is the reference chemical potential of bulk Te:

$$E_f(\Delta\mu_{\mathrm{Te}}) = E_f^0 + \tfrac{1}{2}\Delta G_f^0 \Delta n_{\mathrm{Bi}} + \left(\Delta n_{\mathrm{Te}} - \tfrac{3}{2}\Delta n_{\mathrm{Bi}}\right)\Delta\mu_{\mathrm{Te}}. \qquad (4)$$

A corresponding expression can be written for the formation energy as a function of $\Delta\mu_{\mathrm{Bi}}$. Equations (2) and (3) also fix bounds on the values of μ_{Te}, and μ_{Bi}, which ensure that Bi_2Te_3 is maintained stable against elemental precipitation in the range of conditions from Te-rich (Bi-poor) to Te-poor (Bi-rich):

$$\tfrac{1}{2}\Delta G^0 \leqslant \Delta\mu_{\mathrm{Bi}} \leqslant 0, \qquad (5)$$

$$\tfrac{1}{3}\Delta G^0 \leqslant \Delta\mu_{\mathrm{Te}} \leqslant 0. \qquad (6)$$

Notice that according to Eq. (1), the formation energy of the exchange-pair defects $X_{\mathrm{Bi\text{-}Te1}}$ and $X_{\mathrm{Bi\text{-}Te2}}$ do not depend on the values of the chemical potentials.

III. RESULTS AND DISCUSSION

A. Structure optimization

The lattice structures of ideal elemental bulk Bi and Te, as well as that of Bi_2Te_3, were calculated. This is a prerequisite to obtaining proper estimates of defect formation energies using Eq. (1). The optimal lattice parameters are found by minimization of the total energy as a function of both lattice parameters and internal coordinates. The results of the calculations are summarized and compared to experimental data and other theoretical calculations in Table I. In spite of omitting spin-orbit coupling and the known systematic LDA underestimation of the lattice parameters and unit-cell volume, a good agreement of our calculated optimal lattice parameters for Bi, Te, and Bi_2Te_3 with the corresponding experimental data is obtained. Due to the fitting process, some lattice parameters are slightly overestimated, but the total volume of the unit cell, $\sqrt{3}\, a^2c/2$, is underestimated by 2.2% for Bi, by 6.7% for Te, and by 2.1% for Bi_2Te_3. We note that a good agreement for the internal coordinates was obtained only by explicit inclusion of the semicore d states as valence states in our pseudopotentials. When using a pseudopotential with the d states in the core, the internal coordinates were off such that the Te1-Te1 interaction was underestimated and the layered quintuple structure was not obtained. All calculations are therefore done with the pseudopotentials with d states treated as valence states. Our calculated lattice parameters are also in agreement with previous theoretical calculations based on the LDA for Te by Kresse *et al.*[32] and by Kirchhoff *et al.*,[33] and for Bi by Díaz-Sánchez *et al.*[30] For Bi_2Te_3 our calculated lattice parameters are also in agreement with the calculations by Wang and Cagin[35] who used a generalized gradient approximation (GGA) with the Teter-Pade parametrization for exchange and correlation.

The various defects, namely vacancies, antisite, and exchange-pair defects, are introduced into the ideal bulk hexagonal $2 \times 2 \times 1$ Bi_2Te_3 system, and the system is relaxed until all forces are smaller than 0.05 eV/Å. In all cases, most atoms relaxed only slightly from their perfect bulk equilibrium positions, by at most 0.05 Å. The largest relaxations occurred for antisite defect pairs in the van der Waals gap, i.e., antisite pairs of $\mathrm{Bi_{Te1}}$ and exchange pairs $X_{\mathrm{Bi\text{-}Te1}}$. The atoms in the gap relaxed out of plane into the gap, causing a reduction of the gap width from the ideal Te1-Te1 distance of 3.58 Å by at most 0.15 Å.

B. Vacancies and antisite defects

The results for the formation energies for vacancies and antisite defects calculated according to Eq. (1) as a function of $\Delta\mu_{\mathrm{Te}}$ and $\Delta\mu_{\mathrm{Bi}}$ are shown in Fig. 3 and are summarized in Tables II and III for Bi-rich, and Te-rich conditions, respectively. The atom indices in the tables refer to those shown in Fig. 2. In addition to calculations with a single defect in the hexagonal $2 \times 2 \times 1$ supercell, calculations with pairs of defects within the same supercell are performed. The pairs of

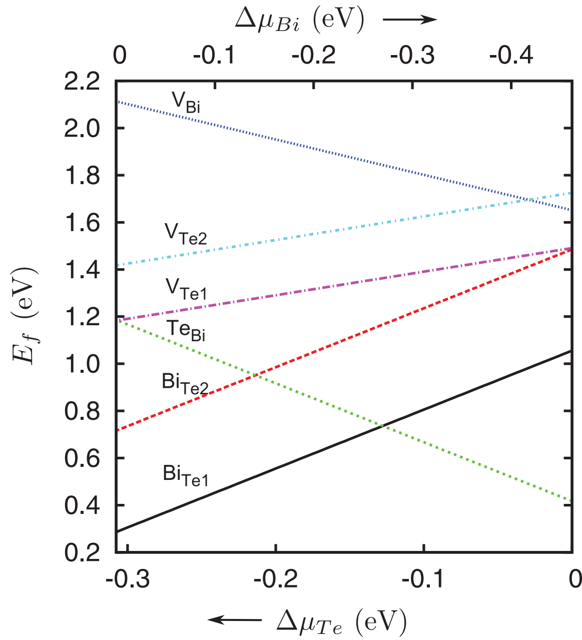

FIG. 3. (Color online) The formation energy of the vacancy and antisite defects in Bi_2Te_3 as a function of the chemical potentials of Te (bottom axis) and Bi (upper axis).

defects were introduced at different separations as indicated in Tables II and III, to allow an estimate of the effect of system size and PBC on the calculated formation energies. The formation energy, to within the obtained numerical accuracy, turns out to be practically independent of the separation between the defects. The hexagonal $2 \times 2 \times 1$ system is therefore large enough that defects in each supercell are effectively screened from their own images. This was demonstrated also for the case of Sb_2Te_3 by Thonhauser *et al.*[28] As depicted in Fig. 3 and Tables II and III, the vacancy formation energies are consistently larger than the antisite-defect formation energies. For vacancies on the Te2 sublattice the formation energy is higher than that for vacancies on the Te1 sublattice. This lower vacancy formation energy of V_{Te1} may be a explained as a result of the weak Te1-Te1 bond and of the larger separation between the quintuple blocks. Vacancies on the Bi sublattice have the highest formation energy at all conditions. A surprising result is that even for Te-rich conditions, where one expects vacancies on the Bi sublattice to be dominating, V_{Te1} still has the lowest vacancy formation energy.

TABLE II. The formation energies E_f for vacancies at Bi-rich ($\Delta\mu_{Bi} = 0$) and Te-rich conditions ($\Delta\mu_{Te} = 0$). The indices refer to the atoms removed according to Fig. 2; d is either the closest distance of a defect and its nearest periodic image in the case of systems with only one defect, or the closest distance between the defects in the case of a pair of defects.

			E_f (eV)	
System	Index	d (Å)	Bi-rich	Te-rich
V_{Bi}				
1	25	8.78	2.11	1.65
2	25–37	5.95	2.13	1.67
3	45–20	14.8	2.15	1.69
V_{Te1}				
1	13	8.78	1.18	1.49
2	13–49	12.45	1.20	1.51
3	29–36	5.66	1.20	1.50
V_{Te2}				
1	1	8.78	1.42	1.73
2	21–44	11.14	1.48	1.79

TABLE III. The formation energies E_f for antisite defects at Bi-rich ($\Delta\mu_{Bi} = 0$) and Te-rich conditions ($\Delta\mu_{Te} = 0$). The indices refer to the atoms removed according to Fig. 2; d is either the closest distance of a defect and its nearest periodic image, in the case of systems with only one defect, or the closest distance between the defects in case of a a pair of defects.

			E_f (eV)	
System	Index	d (Å)	Bi-rich	Te-rich
Te_{Bi}				
1	25	8.78	1.19	0.42
2	25–37	5.95	1.19	0.42
3	45–20	14.8	1.20	0.43
Bi_{Te1}				
1	13	8.78	0.29	1.06
2	13–49	12.45	0.29	1.06
3	29–36	5.66	0.27	1.04
Bi_{Te2}				
1	1	8.78	0.72	1.49
2	21–44	11.14	0.70	1.46

The situation for the antisite-defect formation energies is rather different; the type of most stable antisite defect is dependent on the stoichiometry. For Bi-rich conditions, characterized by $\Delta\mu_{Bi} = 0$, the lowest formation energy is the one for Bi_{Te1}, which is 0.4 eV and 0.9 eV lower than the corresponding formation energies for Bi_{Te2} and Te_{Bi}, respectively. This indicates that for Bi-rich conditions the most significant antisite defect is Bi_{Te1}. On the other hand for Te-rich conditions, the lowest formation energy is obtained for Te_{Bi} which is 0.7 eV and 1.1 eV lower than the corresponding formation energies of Bi_{Te1} and Bi_{Te2}, respectively. This means that for Te-rich conditions, Te_{Bi} is the dominating defect in the system.

Horák *et al.*,[22] suggested, based on experimental data, the formation of Bi_{Te} antisite defects for small concentrations of Bi overstoichiometry, while Frangis *et al.*,[25] observed that lamellae of seven or nine layers (instead of five) become preferable. This supports our finding that vacancies cannot compensate for the excess of Bi in the system due to their high formation energy in the whole range of allowed chemical potentials. Hence point defects which essentially preserve the main framework of the tetradymite structure, but which allow for a change in the occupation by antisite defects, would be more probable than vacancies.

We therefore conclude that vacancies are not likely to play an important role for the thermoelectric properties of the system. This is further manifested by considering that the calculated formation energy per formula unit of the Bi_2Te_3 composed from elemental Bi and Te is found to be 0.92 ± 0.05 eV (experimental enthalpies of formation are

found to be in the range 0.41–0.83 eV[48]), which is lower than the calculated energy of formation of vacancies. This may explain the extrusion of Te out of Bi_2Te_3 from the system observed experimentally[10,20,23] upon increasing the Te concentration. It is energetically much more favorable for the system to disintegrate rather than to accommodate the excess Te and the associated V_{Bi} vacancies.

This also poses some challenges in particular on previously proposed point-defect models[14–16] that rely on the formation of vacancies on the Bi and Te sublattices as the main compensator mechanism for antisite Bi_{Te} defects under Bi-rich conditions. On the other hand, it supports those models suggesting that the charge carrier density is determined solely based on the formation of antisite defects.[10,18,20,25]

C. Exchange antisite defect pairs

Although our model is based on the dilute limit of defects, it is nonetheless useful to calculate the formation energy for a pair of opposite antisite defects which are in close proximity. Table IV presents the results for the exchange pairs $X_{\text{Bi-Te1}}$, with the exchange of a Bi atom with a Te1 atom in the same supercell. For completeness we also included the exchange pairs $X_{\text{Bi-Te2}}$, with the exchange of a Bi with a Te2 atom (see Table V). As expected, the formation energy for $X_{\text{Bi-Te1}}$ is lower than that for $X_{\text{Bi-Te2}}$. Furthermore, the formation energy in either case is almost constant for all pairs which are not direct nearest neighbors (cf. systems No. 1 in Tables IV and V). Similarly to Ref. 28, we may describe the exchange pair as formed by two separate antisite defects. An interaction energy between the separated antisite defects can then be defined as

$$E_i(X_{\text{Bi-Te}}) = E_f(X_{\text{Bi-Te}}) - E_f(\text{Bi}_{\text{Te}}) - E_f(\text{Te}_{\text{Bi}}). \quad (7)$$

The interaction energies are also given in the last column of Tables IV and V. It can be seen that apart from nearest-neighbor exchange pairs, the interaction energies are very small. Only for nearest-neighbor Bi-Te exchange pairs, the formation energy is substantially lower than the sum of the formation energies of the corresponding isolated antisite defects. We believe this to be a result of efficient screening typically found in small-band-gap semiconductors as in metallic systems. The nearest-neighbor $X_{\text{Bi-Te1}}$ exchange pair is bound particularly strongly: The binding energy is about 0.5 eV, which is comparable to the formation energies of antisite defects. Exchange pairs are therefore strongly bound in the system when they are on nearest-neighbor sites, and as such should be considered effectively as a defect couple. We also note that the nearest-neighbor exchange pair also leads to the formation of a seven-layer lamella, with one normal five-layer lamella, and a layer composed of only three atoms [Te1-Bi-Te1]. The low energy of the nearest-neighbor $X_{\text{Bi-Te1}}$ may therefore be an indicator for the feasibility of the seven-layer structures observed by Frangis *et al.*[25]

TABLE IV. The formation energies for exchange antisite pair $X_{\text{Bi-Te1}}$ and the interaction energy E_i calculated relative to separated antisites. The indices refer to the Bi atoms replaced according to Fig. 2. The replaced Te atom is No. 13 in Fig. 2.

System	Index	Distance (Å)	E_f (eV)	E_i (eV)
1	19	3.04	0.98	−0.49
2	7	4.8	1.39	−0.08
3	25	5.87	1.31	−0.16
4	57	8.5	1.40	−0.07
5	37	11.66	1.30	−0.17
6	48	14.25	1.40	−0.08

TABLE V. The formation energies for exchange antisite pair $X_{\text{Bi-Te2}}$ and the interaction energy E_i calculated relative to separated antisites. The indices refer to the Bi atoms replaced according to Fig. 2. The replaced Te atom is No. 1 in Fig. 2.

System	Index	Distance (Å)	E_f (eV)	E_i (eV)
1	5	3.01	1.54	−0.36
2	6	5.46	1.78	−0.12
3	45	8.28	1.78	−0.12
4	18	9.17	1.66	−0.24
5	25	11.92	1.81	−0.09
6	26	12.73	1.81	−0.09

D. Electronic structure analysis

The thermoelectric properties are certainly influenced by the electronic and thermal properties of the material. In the following we consider the bulk electronic structure and changes therein caused by the most probable point defects, i.e., the ones with the lowest formation energies. The analysis is done by means of total and partial (site- and angular-momentum-projected) densities of electronic states (PDOSs). The total and partial DOSs for an ideal bulk Bi_2Te_3 crystal are shown in Fig. 4, as calculated both with the hexagonal $2 \times 2 \times 1$ supercell and the rhombohedral unit cell. The total DOSs (top panel) coincide very well, demonstrating the reasonable equivalence of the k-point meshes as described in Sec. II A. The spin-orbit coupling was not included in our

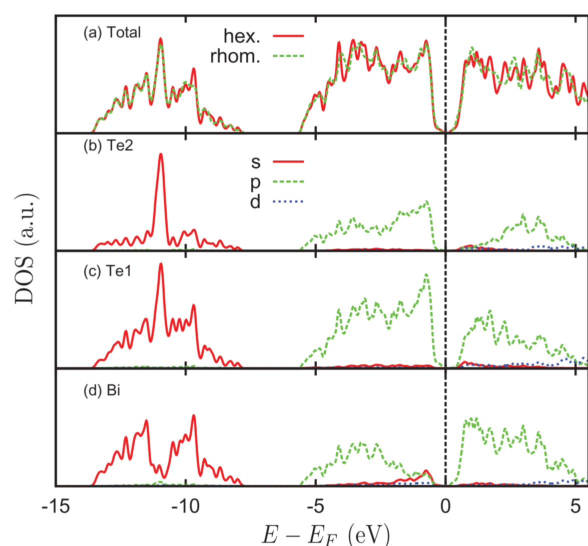

FIG. 4. (Color online) Total densities of states for Bi_2Te_3 (a) comparing the DOS calculated for the hexagonal and rhombohedral unit cells, and the partial DOS from (b) Te2, (c) Te1, and (d) Bi atoms.

calculations. However this was shown to have a negligible effect on the PDOSs,[49,50] as can be seen as well by comparing our PDOSs in Fig. 4 with results of previous calculations which included spin-orbit interaction; see, e.g., Fig. 4 in Ref. 49. We note that from Fig. 4 no information regarding the band gap can be extracted. We have conducted a further calculation of the total DOS using the rhombohedral bulk unit cell of Bi_2Te_3 with a very dense Monkhorst-Pack mesh of $32 \times 32 \times 32$ k points, employing the linear tetrahedron method for Brillouin-zone summations.[51] This gave a band gap of 0.097 eV, which is underestimated by about 30% with respect to the experimental value of 0.13 eV,[11] as expected from LDA.

Referring to the DOSs in Fig. 4, it is found that the valence and conduction bands consist mainly of p-orbitals only. In the region near the lower conduction band, the Bi-p and, to a lesser extent, Te2-p states dominate, while for the region near the upper valence band, the Te1-p states are dominating, in agreement with previous calculations.[49,50,52] Larson and Lambrecht[50] suggested that n-type transport is primarily influenced by the Bi-p states in the conduction band, while Te1-p valence states contribute the most to the p-type conduction. This is also approximately in line with the model of formal charges, or ionic-like bonding for Bi_2Te_3.[15,16,22] Namely, Te is assumed to gain two electrons, to close the p shell, while each Bi atom is assumed to give up three of its valence electrons. However, the electronegativity of Te is only slightly larger than that of Bi ($X_{\mathrm{Bi}} = 1.9$, $X_{\mathrm{Te}} = 2.1$[53]), which would, as suggested by the calculated DOSs in Fig. 4, result in metallic bonding, in agreement also with the tight-binding calculations of Pecheur and Toussiant.[27] Nevertheless, the results suggest that Te1 would contribute electrons while Bi would contribute holes to the charge carriers; i.e., Te is expected therefore to be a donor and Bi an acceptor. The s states are about 10 eV below the Fermi level and hence do not play any significant role in bonding or transport properties.

The site-projected densities of states for the antisite defects are shown in Fig. 5. There are two main effects, the first one is the shift of the Fermi level into the valence band in the case of Bi_{Te1} and Bi_{Te2}, or into the conduction band in the case of Te_{Bi}. The second effect is the appearance of a sharp peak at the band-gap edges, corresponding to the formation of a flat-band defect level, which in the case of Bi_{Te1} and Bi_{Te2} is an acceptor level at the valence band edge, leading to p-type conduction, while in the case of Te_{Bi} is a donor level at the conduction band edge, leading to n-type conduction. The antisite defects lead therefore to charge carriers with heavy effective masses, which would affect the transport and hence the thermoelectric properties in a profound way. Only very small changes to the PDOSs of the other atoms which are more distant from the defect in the unit cell were found, suggesting that the antisite defects have only a short-ranged effect on the electronic structure. For the case of an exchange antisite defect pair, the site-projected DOSs are shown in Fig. 6 for the exchange on nearest-neighbor Bi and Te1 sites (cf. exchange No. 1 in Table IV). Compared to the PDOSs of the separated antisite defect pairs in Figs. 5(a) and 5(c), the peaks corresponding to the flat defect bands are lower, and due to stoichiometry, there is no shift of the Fermi level, indicating that in this case, no net contribution to the charge carrier concentration exists, as expected.

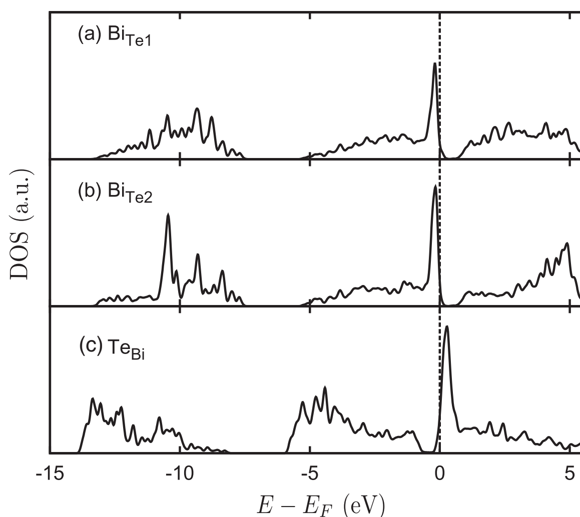

FIG. 5. The site-projected DOS for individual (a) Bi_{Te1}, (b) Bi_{Te2}, and (c) Te_{Bi} antisite defects.

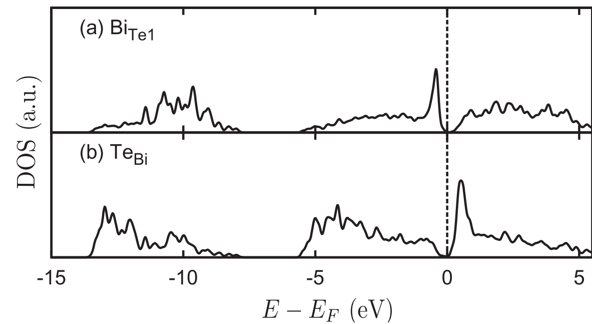

FIG. 6. The site-projected DOS for (a) Bi_{Te1} and (b) Te_{Bi} of the $X_{\text{Bi-Te1}}$ nearest-neighbor exchange pair defect.

A closer look at the defect levels is given in Fig. 7, where the total DOS is shown near the Fermi level for the perfect bulk, Bi_{Te1}, and Te_{Bi}, and for exchange antisite defect pair (No. 1 in Table IV) systems. The total DOSs of the defect systems are shifted so that the core states (not shown) coincide with that of the perfect bulk system. As seen in Fig. 7, the defect levels cause an increase of the DOS at the top of the valence band for the case of Bi_{Te1} antisite defects, and at the bottom of the conduction band for Te_{Bi} antisite defects. Furthermore, these defect states clearly overlap the valence

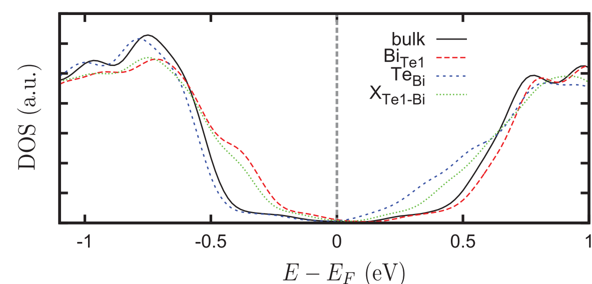

FIG. 7. (Color online) The total DOS near the Fermi energy of the perfect bulk, Bi_{Te1}, and Te_{Bi}, and of the $X_{\text{Bi-Te1}}$ nearest-neighbor exchange pair defect.

band states for Bi_{Te} and the conduction band states for Te_{Bi}. This may suggest that these defect states are resonance states, which contribute to the energy and charge transport, and may lead to an enhanced thermopower factor. Although the *k*-point sampling, broadening, and neglect of spin-orbit coupling, as well as the effectively high density of defects imposed by the periodic boundary conditions, may affect the positions of the peaks, the appearance of such pronounced features in the DOS strongly suggests that these are indeed resonance defect states rather than deep or shallow defect states in the band gap.

IV. SUMMARY AND CONCLUSIONS

We have a studied the most prominent point defects in the thermoelectric material Bi_2Te_3. The formation energies of vacancies on the Bi, Te1, and Te2 sublattices have been calculated from first principles based on the *ab initio* thermodynamics formalism. The electronic structure effects were studied by means of the projected densities of electronic states (PDOSs). We find, in contradiction to several previous point-defect models,[14–16,19,21,22] that vacancies in Bi_2Te_3 are not expected to play a significant role for the thermoelectric properties of Bi_2Te_3. The most dominant defects are antisite defects on both the Te1 and Bi sublattices, where Bi_{Te1} is dominant at Bi-rich conditions, while Te_{Bi} is dominant for Te-rich conditions. Near stoichiometry both antisite defects may be equally probable. The existence of antisite defects has a profound impact on the band structure of Bi_2Te_3; flat defect bands, which are likely resonances, are formed near the bulk band edges. For Bi_{Te}, the defect levels lie at the top of the valence band, and thus may act as acceptor levels leading to *p*-type conduction. For Te_{Bi}, the defect levels lie at the bottom of the conduction band, and thus may act as donor levels leading to *n*-type conduction. We show that growth conditions may lead to either Bi_{Te} or Te_{Bi} antisite defects, as depicted by the dependence of their formation energies on the chemical potentials. This explains the observed sensitivity of charge carrier type and thermopower of Bi_2Te_3-based thermoelectric materials on the growth conditions.[6–10,14]

Entropy contributions to the formation energies, most notably configuration entropy, have not been included in the present model. Nevertheless the large formation energy difference between the vacancies and antisite defects indicates that our conclusions are unlikely to be altered by including entropy. Another limitation of our current model is that defects are assumed to be charge neutral. For a semiconducting system with a small band gap, this is also not expected to have a crucial influence.

ACKNOWLEDGMENTS

The authors acknowledge financial support from the German Research Foundation (DFG) through the Priority Program SPP1386 "Nanostrukturierte Thermoelektrika" (Projekt EL155/23-1).

---

*adham.hashibon@iwm.fraunhofer.de

[1] H. J. Goldsmid, *Thermoelectric Refrigeration* (Plenum, New York, 1964).
[2] A. F. Ioffe, *Semiconductor Thermoelectric and Thermoelectric Cooling* (Infosearch, London, 1957).
[3] Y. Zhao, J. S. Dyck, B. M. Hernandez, and C. Burda, J. Am. Chem. Soc. **132**, 4982 (2010).
[4] X. Yan, B. Poudel, Y. Ma, W. S. Liu, G. Joshi, H. Wang, Y. Lan, D. Wang, G. Chen, and Z. F. Ren, Nano Lett. **10**, 3373 (2010).
[5] Y. Ma, Q. Hao, B. Poudel, Y. Lan, B. Yu, D. Wang, G. Chen, and Z. Ren, Nano Lett. **8**, 2580 (2008).
[6] N. Peranio and O. Eibl, J. Appl. Phys. **103**, 024314 (2008).
[7] D. G. Ebling, A. Jacquot, H. Böttner, L. Kirste, J. Schmidt, and M. Aguirre, J. Electron. Mater. **38**, 1450 (2009).
[8] J. König, M. Winkler, S. Buller, W. Bensch, U. Schürmann, L. Kienle, and H. Böttner, J. Electron. Mater. **40**, 1266 (2011).
[9] R. Venkatasubramanian, E. Siivola, T. Colpitts, and B. O'Quinn, Nature (London) **413**, 579 (2001).
[10] S. Cho, Y. Kim, A. DiVenere, G. K. Wong, J. B. Ketterson, and J. R. Meyer, Appl. Phys. Lett. **75**, 1401 (1999).
[11] R. Sehr and L. R. Testardi, J. Phys. Chem. Solids **23**, 1219 (1962).
[12] J. R. Drabble and C. H. L. Goodman, J. Phys. Chem. Solids **5**, 142 (1958).
[13] R. W. G. Wyckoff, *Crystal Structures 2* (J. Wiley and Sons, New York, 1964).
[14] P. Lošt'ák, Č. Drašar, D. Bachan, L. Beneš, and A. Krejčová, Radiat. Eff. Defects Solids **165**, 211 (2010).
[15] J. Bludská, I. Jakubec, Č. Drašar, P. Lošt'ák, and J. Horák, Philos. Mag. **87**, 325 (2007).
[16] Č. Drašar, P. Lošt'ák, and C. Uher, J. Electron. Mater. **39**, 2162 (2010).
[17] D. L. Medlin, Q. M. Ramasse, C. D. Spataru, and N. Y. C. Yang, J Appl. Phys. **108**, 043517 (2010).
[18] C. B. Satterthwaite and R. W. Ure, Phys. Rev. **108**, 1164 (1957).
[19] G. Miller and C.-Y. Li, J. Phys. Chem. Solids **26**, 173 (1965).
[20] R. F. Brebrick, J. Phys. Chem. Solids **30**, 719 (1969).
[21] J. Horák, K. Cermák, and L. Koudelka, J. Phys. Chem. Solids. **47**, 805 (1986).
[22] J. Horák, J. Navrátil, and Z. Starý, J. Phys. Chem. Solids **53**, 1067 (1992).
[23] L. W. da Silva, M. Kaviany, and C. Uher, J. Appl. Phys. **97**, 114903 (2005).
[24] T. C. Harman, B. Paris, S. E. Miller, and H. L. Goering, J. Phys. Chem. Solids **2**, 181 (1957).
[25] N. Frangis, S. Kuypers, C. Manolikas, G. V. Tendeloo, J. V. Landuyt, and S. Amelinckx, J. Solid State Chem. **84**, 314 (1990).
[26] N. W. Ashcroft and N. D. Mermin, *Solid State Physics* (Saunders College, Philadelphia, 1976).
[27] P. Pecheur and G. Toussaint, J. Phys. Chem. Solids **55**, 327 (1997).
[28] T. Thonhauser, G. S. Jeon, G. D. Mahan, and J. O. Sofo, Phys. Rev. B **68**, 205207 (2003).
[29] C. G. Van de Walle and J. Neugebauer, J. Appl. Phys. **95**, 3851 (2004).

[30] L. E. Díaz-Sánchez, A. H. Romero, and X. Gonze, Phys. Rev. B **76**, 104302 (2007).
[31] P. Cucka and C. S. Barrett, Acta Crystallogr. **15**, 865 (1962).
[32] G. Kresse, J. Furthmüller, and J. Hafner, Phys. Rev. B **50**, 13181 (1994).
[33] F. Kirchhoff, N. Binggeli, G. Galli, and S. Massidda, Phys. Rev. B **50**, 9063 (1994).
[34] R. Keller, W. B. Holzapfel, and H. Schulz, Phys. Rev. B **16**, 4404 (1977).
[35] G. F. Wang and T. Cagin, Phys. Rev. B **76**, 075201 (2007).
[36] C. Elsässer, N. Takeuchi, K. M. Ho, C. T. Chan, P. Braun, and M. Fähnle, J. Phys. Condens. Matter **2**, 4371 (1990).
[37] K. M. Ho, C. Elsässer, C. T. Chan, and M. Fähnle, J. Phys. Condens. Matter **4**, 5189 (1992).
[38] B. Meyer, C. Elsässer, F. Lechermann, and M. Fähnle, Fortran90 Program for Mixed-Basis Pseudopotential Calculations for Crystals (unpublished).
[39] D. M. Ceperley and B. J. Alder, Phys. Rev. Lett. **45**, 566 (1980).
[40] J. P. Perdew and A. Zunger, Phys. Rev. B **23**, 5048 (1981).
[41] D. R. Hamann, M. Schlüter, and C. Chiang, Phys. Rev. Lett. **43**, 1494 (1979).
[42] D. Vanderbilt, Phys. Rev. B **41**, 7892 (1990).
[43] H. J. Monkhorst and J. D. Pack, Phys. Rev. B **13**, 5188 (1976).
[44] C. L. Fu and K. M. Ho, Phys. Rev. B **28**, 5480 (1983).
[45] C. Elsässer, M. Fähnle, C. T. Chan, and K. M. Ho, Phys. Rev. B **49**, 13975 (1994).
[46] W. Körner and C. Elsässer, Phys. Rev. B **81**, 085324 (2010).
[47] S. Körbel, P. Marton, and C. Elsässer, Phys. Rev. B **81**, 174115 (2010).
[48] S. A. Humphry-Baker and C. A. Schuh, Scripta Mater. **65**, 516 (2011).
[49] S. K. Mishra, S. Satpathy, and O. Jepsen, J. Phys. Condens. Matter. **9**, 461 (1997).
[50] P. Larson and W. R. L. Lambrecht, Phys. Rev. B **78**, 195207 (2008).
[51] P. E. Blöchl, O. Jepsen, and O. K. Andersen, Phys. Rev. B **49**, 16223 (1994).
[52] B.-L. Huang and M. Kaviany, Phys Rev. B **77**, 125209 (2008).
[53] D. R. Lide, ed., *CRC Handbook of Chemistry and Physics*, 89th ed. (CRC Press, Boca Raton, FL, USA, 2009), Chap. 9, p. 98.